# Tribocorrosion Behaviour of Ti–6Al–4V Alloy in Biomedical Implants: Effects of Applied Load and Surface Roughness on Material Degradation

Ali Sabea Hammood[1] · L. Thair[2] · Hanaa Diab Altawaly[1] · Nader Parvin[3]

## Abstract

Tribocorrosion covers the science of surface transformations resulting from the interaction of mechanical loading and chemical reactions that occur between elements of a tribosystem exposed to corrosive environments. Implant materials are subjected to relative movements, which can cause wear damage, together with corrosive attack of the body fluids. Ti–6Al–4V alloy has been widely used for this purpose due to its superior biocompatibility and excellent corrosion resistance and good mechanical properties. The purpose of this work is to evaluate the tribocorrosion of Ti–6Al–4V alloy under different load and surface conditions. The tribocorrosion tests of Ti–6Al–4V alloy were performed using pin on disc tests at phosphate buffer saline solution (PBS), under various loading (0.5–25) N and surfaces roughness (240, 320, 400, 600) µm grits. Surface morphology, chemical composition and tribocorrosion resistance studied by scanning electron microscopy (SEM), energy-dispersive spectroscopy (EDS) and Tafel potential polarization. The result indicate, by increasing contact load, the smoother surface (600 µm grit) give lower average tribocorrosion current density as compared with surface (320, 240, 400) µm grits suggesting that the damage is more pronounced on the smooth surface.

**Keywords** Ti–6Al–4V alloy · Tribocorrosion · Material degradation · Phosphate buffer saline solution

## 1 Introduction

In the past few decades, the ageing of the population and the change of people's lifestyle, tens of thousands of people have been plagued by orthopedic, oral and maxillofacial diseases. Thus, solving these problems enables patients to return to a better lifestyle, and the demand for medical implants has increased with the growing implant technology [1]. There are varieties of biomaterials such as metallic, ceramics and polymers that have been used as biomedical devices. Metallic biomaterials can be grouped as steels, cobalt and titanium-based alloys [2–4]. The main property required of a biomaterial is that it does not illicit an adverse reaction when placed into services, that means to be a biocompatible material. As well, good mechanical properties, high corrosion resistance and excellent wear resistance are required [5]. Metals are widely used as biomaterials due to their better mechanical characteristics i.e. toughness, high strength, thermal and electrical conductivity [6].

The most preferable titanium alloy is Ti–6Al–4V and covers about 50 percent of complete titanium world construction. Presently, Ti–6Al–4V widely utilized in biomedical industries, automotive, chemical, aerospace and marine [7]. Titanium and its alloys are a fundamental biomedical material, due to their high strength, low weight, and excellent corrosion resistance [8–11]. Titanium and titanium alloys show an exceptional mixture of physical, mechanical and corrosion protection but these materials show poor wear

✉ Ali Sabea Hammood
   alis.altameemi@uokufa.edu.iq

   L. Thair
   phythair2011@gmail.com

   Hanaa Diab Altawaly
   hanaad.altawaly@uokufa.edu.iq

   Nader Parvin
   nparvin@aut.ac.ir

1  Department of Materials Engineering, Faculty of Engineering, University of Kufa, Najaf, Iraq

2  Iraqi Atomic Energy Commission (IAEC), Nuclear Research Center, Baghdad, Iraq

3  Department of Mining and Metallurgical Engineering, Amirkabir University of Technology, Tehran, Iran

resistance, fretting and tribological characteristics. It has been reported that low thermal conductivity of titanium and its alloys lead to poor tribological properties [12–14].

The repeated removal of oxide films produces wear and corrosion products, i.e. wear debris and metal ions. Extensive release of ions from implants can result in adverse biological reactions, and can lead to mechanical failure of the device [15].

In Uhlig's approach, material deterioration resulted from two distinct mechanisms namely: (mechanical wear and wear-accelerated corrosion) According to these mechanisms, the total volume $V_{tot}$ removed by tribocorrosion is given by Eq. (1):

$$V_{tot} = V_{mech} + V_{chem}, \tag{1}$$

where the term $V_{mech}$ represents the metal volume removed by mechanical wear while $V_{chem}$ corresponds to the equivalent metal volume removed by wear-accelerated corrosion [16].

There are four factors of the behavior of electrochemically controlled mechano-electrochemical systems: Electrochemical conditions usual at the rubbing surface metal (applied potential, ohmic resistance, film growth, active dissolution, valence), solution properties in the contact surfaces (viscosity, conductivity, temperature, pH, corrosivity, dissolved oxygen), mechanical/operational condition (normal force, sliding velocity, type of motion, shape and size of contacting bodies) substances and surface characteristics of the specimen (hardness, plasticity, microstructure, inclusions, surface roughness, oxide film properties, wear debris, material transfer) [17, 18].

Tribocorrosion is commonly accepted as an interdisciplinary area of research and such studies on numerous substances are gaining extra consideration by scientists and engineers due to its practical and economical impact [19, 20]. Fretting corrosion is an important subdivision of tribocorrosion, refers to the degradation of a substance subjected to mechanical damage and chemical dissolution due to slight amplitude movement. The tribocorrosion behaviour of medical devices are not yet fully understood [21–24]. The presence of corrosive human solutions leads to fretting damage at the implant bone contact. A tribocorrosion situation where material degradation is caused by immediate presence of micro movements and of an aggressive surroundings [25]. The incidence and severity of fretting-related failures depend on several factors related to mechanically assisted corrosion phenomena. Currently, there is a need to develop and use a test system to systematically control and analyse this processes. The tribocorrosion phenomenon can be deleterious and destructive where by decreasing the life time of the hip implant replacement and causing reactions due to release of debris that can cause toxicity to osteocytes around the stem part of the hip implant. The main objective of this study was

**Table 1** The chemical composition of Ti–6Al–4V alloy

| Material composition | Wt% |
|---|---|
| Titanium | (88.10–90.92) |
| Aluminium | (5.50–6.75) |
| Carbon | (0.08) |
| Iron | (0.4) max |
| Vanadium | (3.5–4.5) |

**Table 2** The chemical composition of PBS solution

| Salt | Concentration (g/L) |
|---|---|
| NaCl | 137 |
| KCl | 2.7 |
| $Na_2HPO_4$ | 10 |
| $KH_2PO_4$ | 1.8 |

to determine the effect of applied load due to human activities and surface roughness conditions on the tribocorrosion of Ti–6Al–4V alloy in biomedical application.

## 2 Experimental Procedure

### 2.1 Materials and Methods

The material which was used in this paper was Ti–6Al–4V alloy. The chemical composition of which is shown in Table 1. This alloy cut into discs of 15 mm in diameter and cone shaped flat-bottomed pins with interface diameter from 1 to 3 mm. Both disc and pin was grinding with different grits (240, 320, 400, and 600) µm. After grinding the sample was cleaned using deionised water to remove any particles on the surface. The pin and disc were fixed in such a way that the grinding scratch lines were perpendicular to each other. The selection of tribocorrosion area approximately 0.385 cm$^2$ and the remaining was covered with nail varnish as a masking cover.

### 2.2 Tribocorrosion System

Tribocorrosion system constituted the cell which acted as the electrochemical environment comprising 60 mL of phosphate-buffered saline (PBS) solution at pH = 7.4 and at 37 °C. The chemical composition of PBS is shown in Table 2. The electrochemical cell also had a central cavity where the samples can be mounted. The disc acted as the working electrode while platinum acted as a counter electrode as well as the reference electrode from saturated calomel electrode in the electrochemical cell. All three
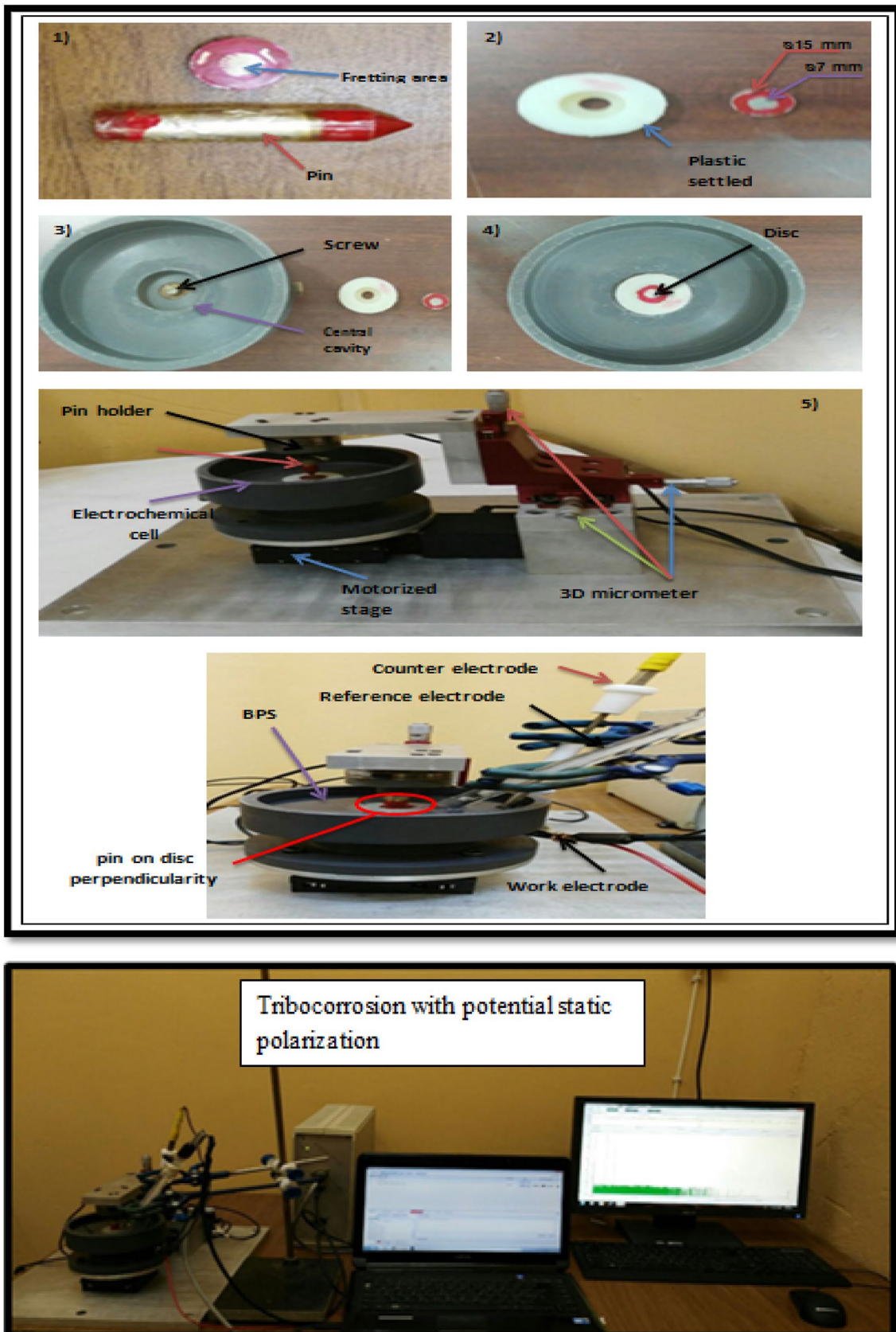
**Fig. 1** Procedure steps for tribocorrosion tests system

**Table 3** The specification of XYZ stage

| Specification | Value |
| --- | --- |
| Maximum speed | 6.5 mm/s |
| Minimum speed | 0.0009302 mm/s |
| Maximum load | 100 N |
| Power supply | 12–16 VDC |
| Motor type | Stepper (2 phase) |
| Weight | 0.59 kg |
| Operating temperature range | 0–50 °C |

electrodes are connected to the potentiostat device type (Winking M Lab 200). The Ti–6Al–4V pin was fixed in the pin holder and three electrodes were also fixed in the system. The corrosion cell was fixed on a motorized stage (linear stage, TL-S28, ZABIR). Table 3 demonstrates the product specifications. The load was varied from 0.5 to 25 N and it is applied on the pin holder during tribocorrosion tests. The pin displacement 2 mm with fretting time 5 min was controlled by simulating device (Zaber Console v2.3.0.3167) between computer and tribocorrosion system. Figure 1 shows steps for tribocorrosion system fixation during the tests.

## 2.3 Scanning Electron Microscopy With Energy-Dispersive Spectroscopy (SEM with EDS)

SEM provides microstructure and morphology details of Ti–6Al–4V alloy before and after tribocorrosion tests. The chemical composition of Ti–6Al–4V alloy specimen surface was analysed by using EDS, which attached to the SEM.

The test accomplished with SEM (SEM-FEI Quanta model, Holland made used at an acceleration voltage of 12.5 kV).

## 3 Results and Discussion

### 3.1 Tribocorrosion

Figure 2 depicts the tribocorrosion for a single step of 240 μm grit at 0.5 N. This Figure demonstrates three regions, the first represents current baseline before tribocorrosion which varies from about 0 to 100 s, The second represents tribocorrosion current which has an amplitude of about 100 to 160 s and the third region corresponds to the recovery of the current baseline. At the beginning of experiments, current increased sharply due to the mechanical distraction of the passive film. When fretting begins, the sharp increase of current is pertained to the mechanical behaviour of the passive film. When the fretting finishes, the current decreases to the qualities were estimated before tribocorrosion because of the regrowth of the passive film layer inside the fretting path.

#### 3.1.1 Effect of Applied Load on Tribocorrosion Behaviour

Figures 3, 4, 5, and 6 show the potentiostatic polarization curve of Ti–6Al–4V alloy in PBS at constant applied potential 500 mV and different applied load from 0.5 N to 25 N to simulate the load change in the human body. It can be seen that due to different levels of current in the figures the fretting is initiated, the current density is increased rapidly and the destruction of the protective layer on the sample
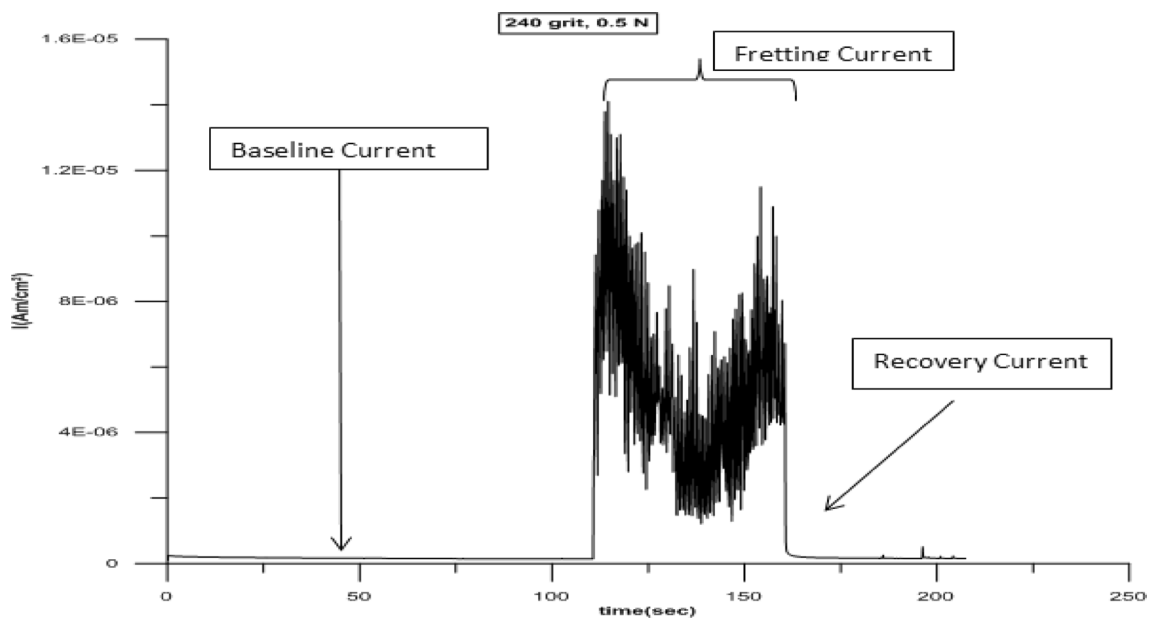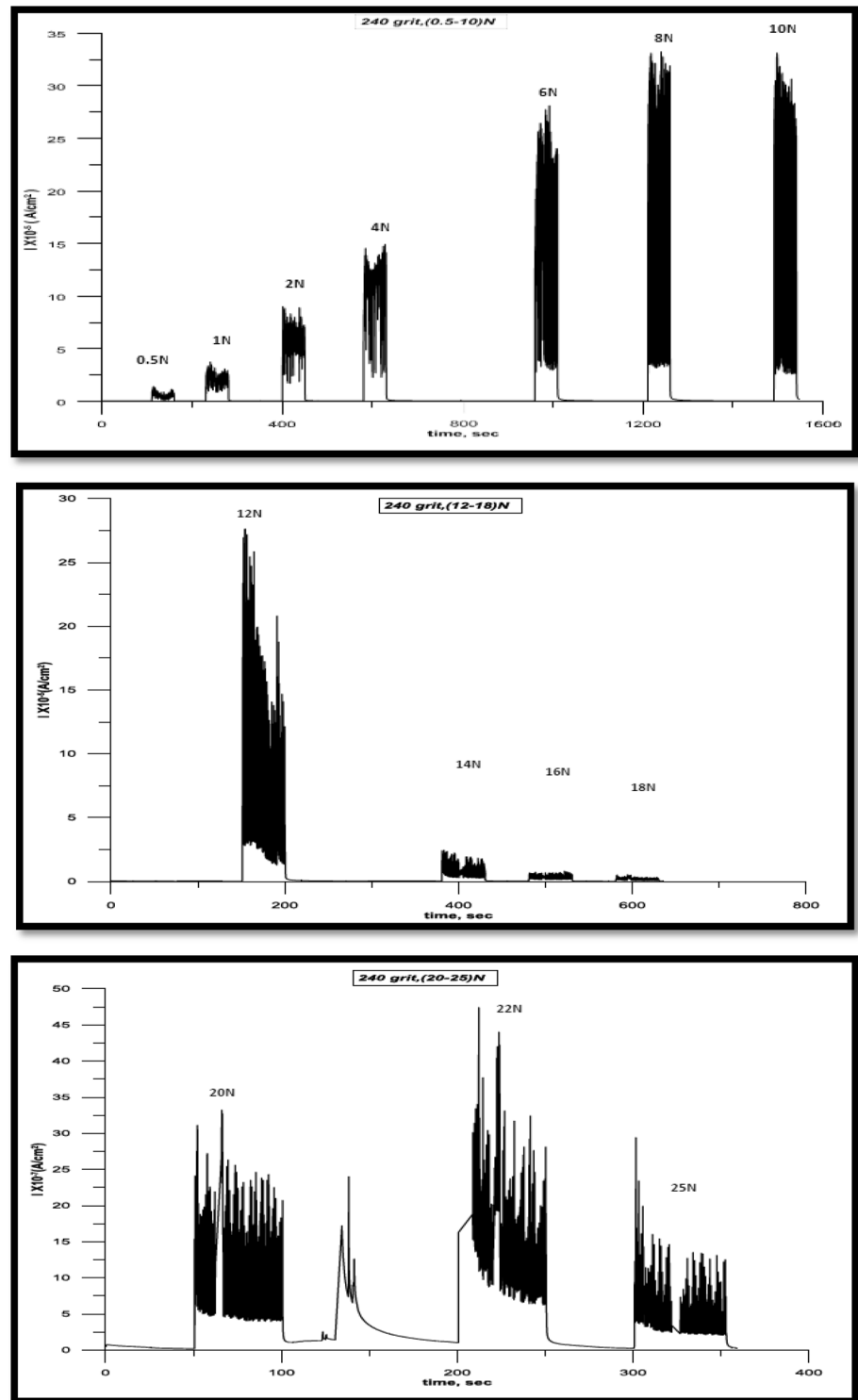


**Fig. 2** Tribocorrosion current density for a single step of 240 μm grit at 0.5 N during tribocorrosion test

**Fig. 3** Current density versus time during tribocorrosion test of Ti–6Al–4V with 240 μm grit surface



surface starts. The current density dropped when the tribocorrosion process stopped. In addition, the generated currents differ with applied load, and indicated a critical current dependence on the applied load. When load increases, currents increase up to a peak value and then currents drop with increasing applied load.

### 3.1.2 Effect of Surface Roughness on Tribocorrosion

The average current density was determined for Ti–6Al–4V alloy according to:

$$I\text{av} = \frac{I\text{max} + I\text{min}}{2} \tag{2}$$

**Fig. 4** Current density versus time during tribocorrosion test of Ti–6Al–4V with 230 μm grit surface
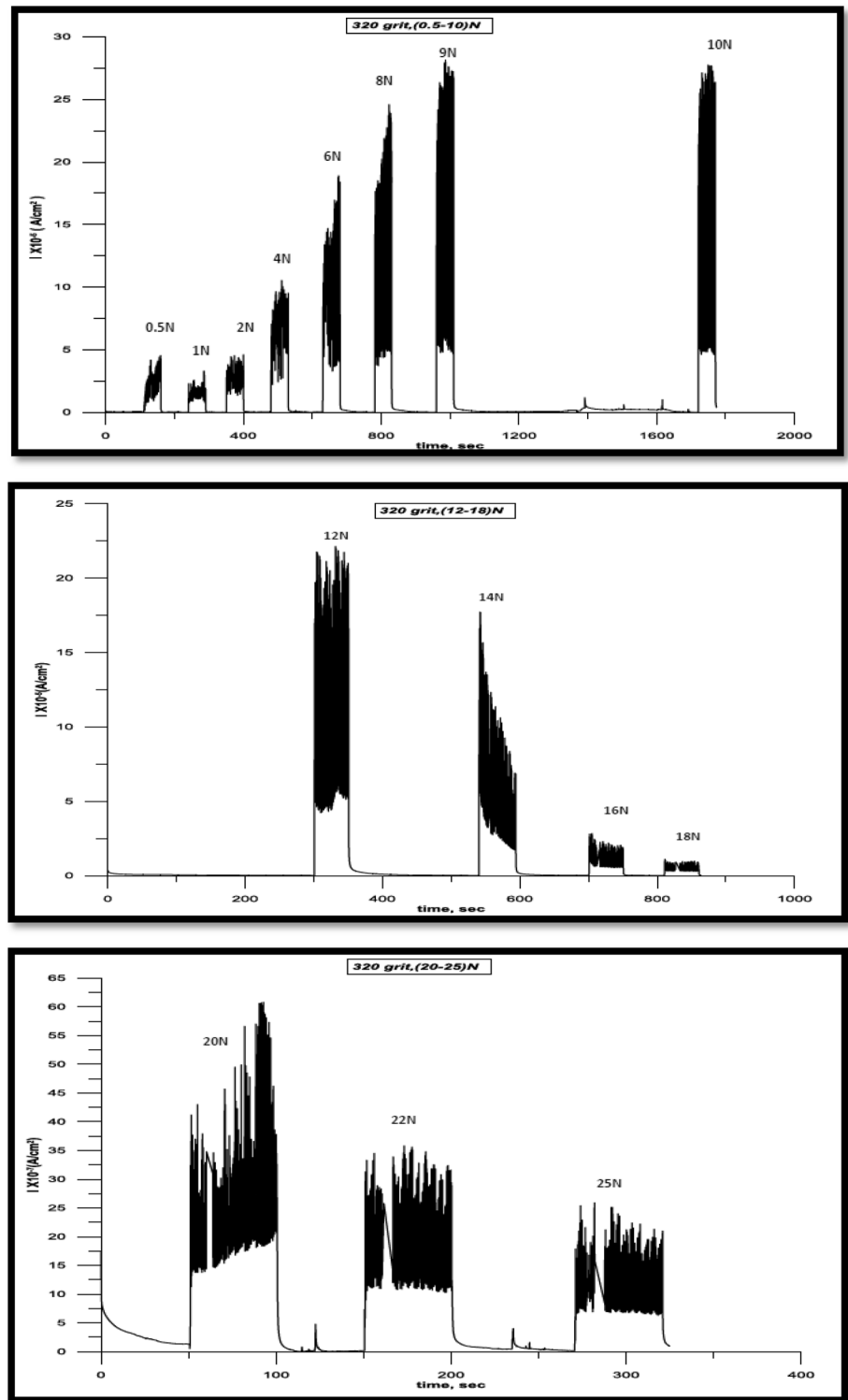


Figure 7 shows average current density versus applied load during tribocorrosion tests for Ti–6Al–4V alloy with different surface roughness condition. There are differences in behaviour of different surfaces based on the roughness,

With increasing contact load, the smooth surface 600 μm gives lower average current density compared with another surface roughness (320, 240 and 400) μm grits. As the applied load increase, the current density increases up to

**Fig. 5** Current density versus time during tribocorrosion test of Ti–6Al–4V with 400 μm grit surface
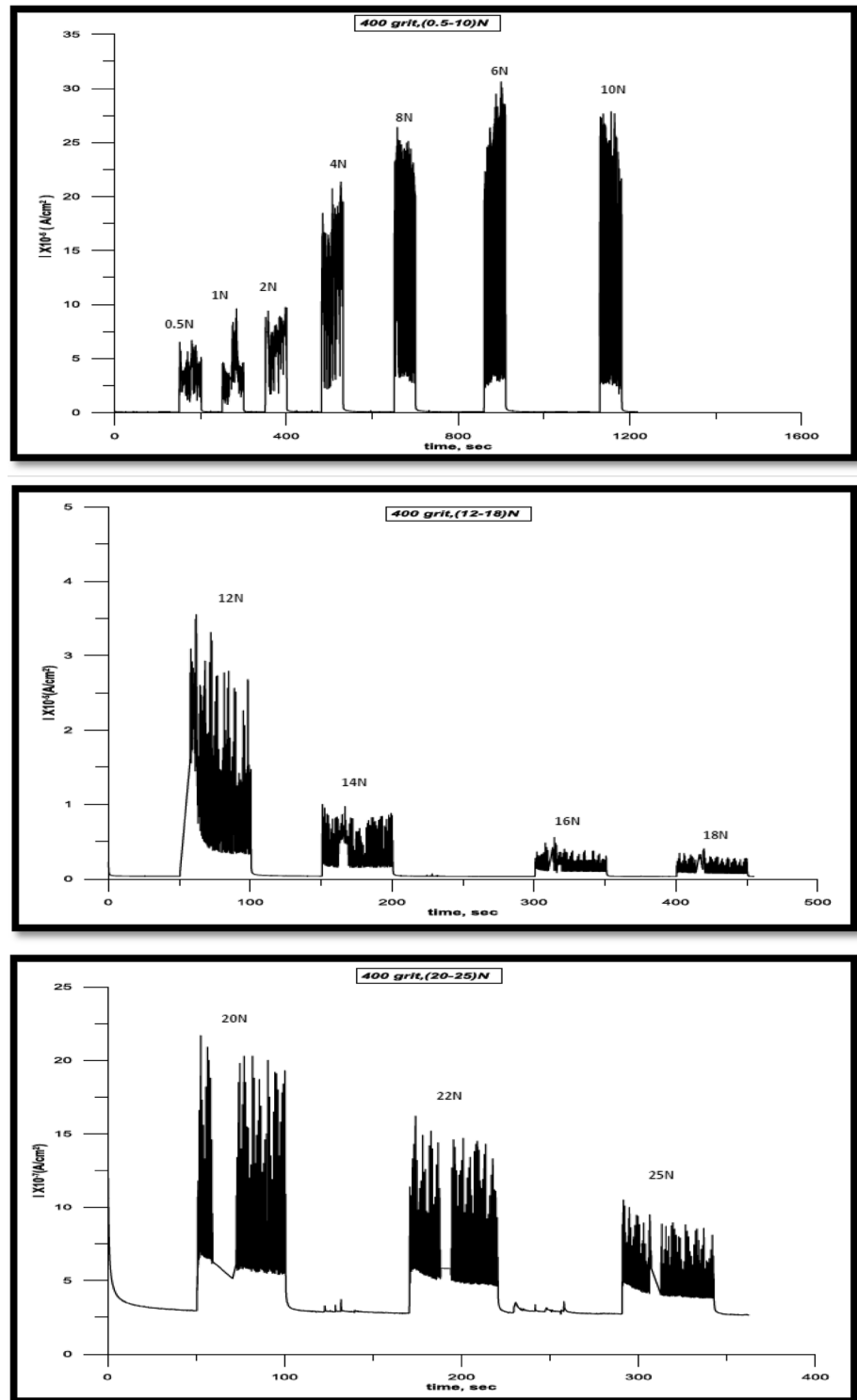


the applied load of 8 N and then further increase in load can lead to decrease in current density so the activation peaks in the first half and lower than those in the second half. The decrease in current during the second half of the run suggests the formation of a partially protective film, perhaps associated with oxidized and compacted wear debris tribomaterial. It also suggests that there is a higher contact stress, which maximizes synergism. The maximum average current density for all surface roughness conditions approximately at 8 N applied load.

**Fig. 6** Current density versus time during tribocorrosion test of Ti–6Al–4V with 600 μm grit surface
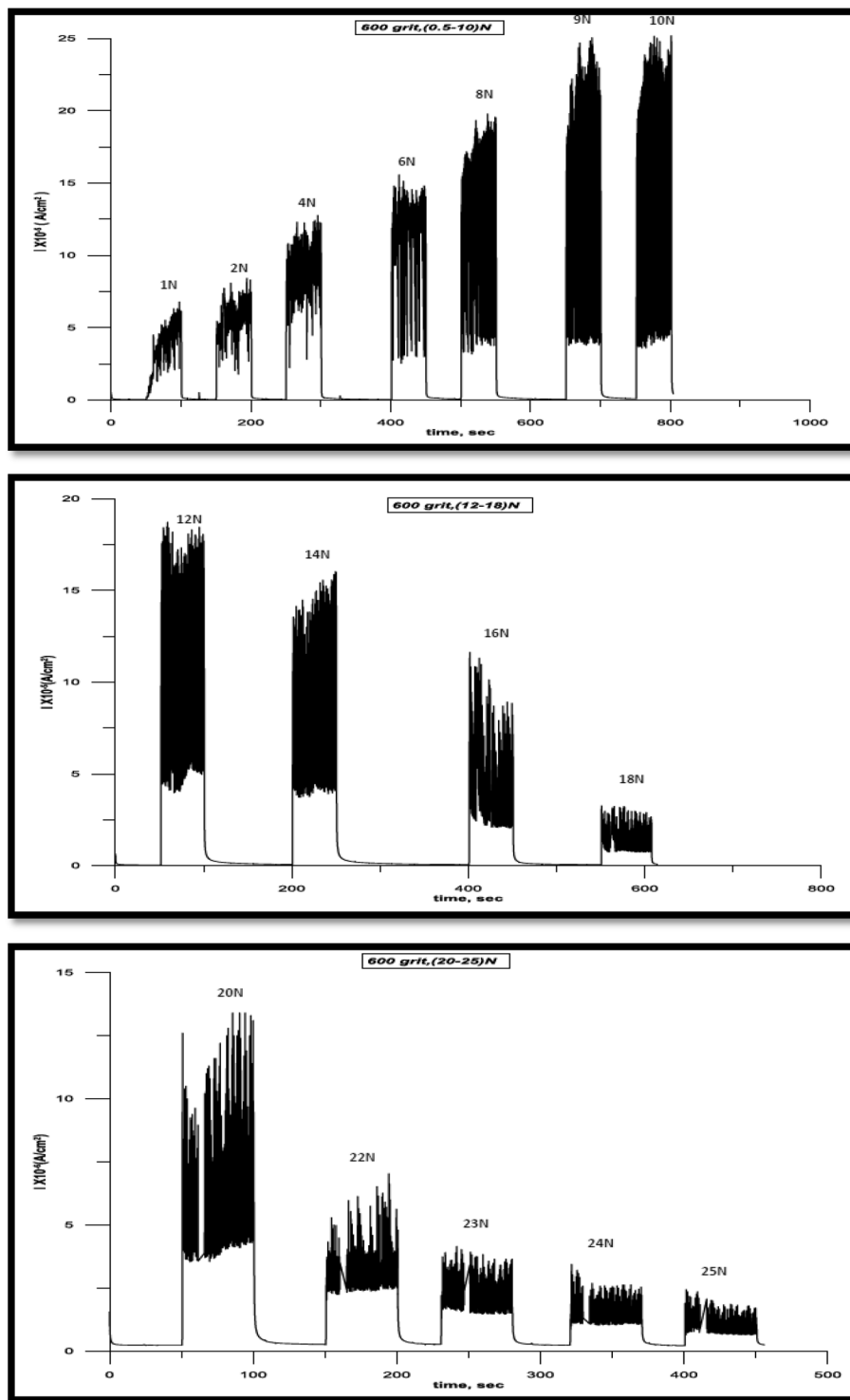


## 3.2 Surface Morphology

SEM micrographs (Fig. 8) showed the tribocorrosion attack on the Ti6Al4 V surface from low surface grit 240 μm to higher surface grit 600 μm grit at 25 N applied load. There are two zones, base zone and fretted zone. Corrosion debris composed mostly of oxide is seen in the fretted zone. The

perpendicularity of the pin is very clear on the disc surfaces during tribocorrosion test. The plastic deformation and ductile behaviour was observed. Grooves and scratches were also observed. Figure 9 illustrates SEM micrographs of samples after tribocorrosion test which pitting corrosion can be observed due to the continuing crevice corrosion when fretting was stopped. Pitting was occurred to a greater degree
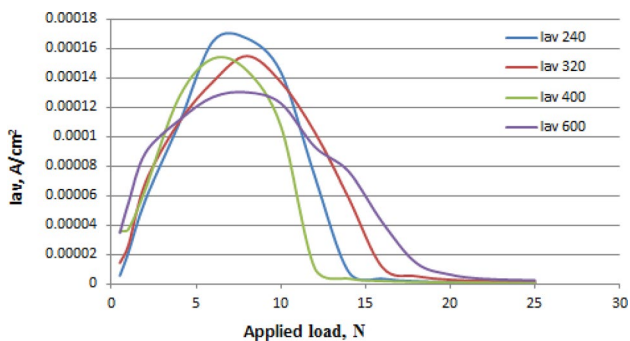
**Fig. 7** Average current density versus applied load during tribocorrosion tests for Ti–6Al–4V alloy with different surface roughness
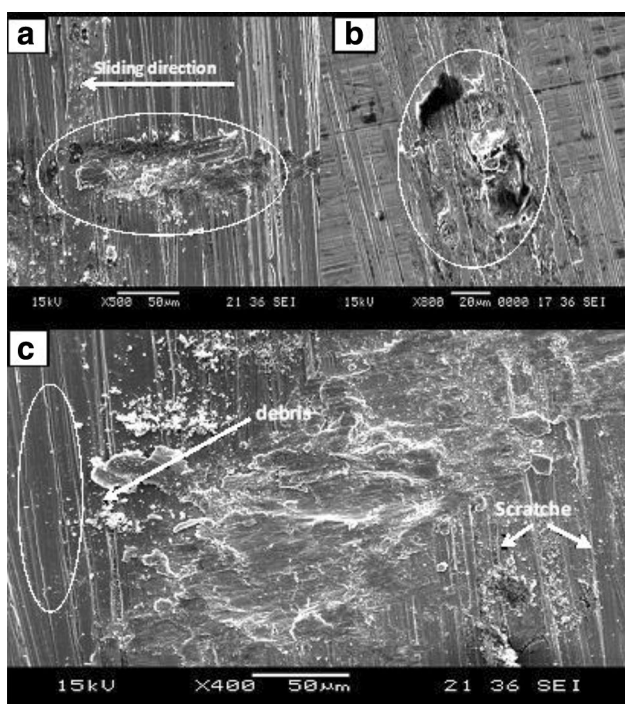


**Fig. 8** SEM micrographs shown the tribocorrosion zone on the Ti–6Al–4V alloy surface, **a** for 240 μm grit, **b** for 600 μm grit and **c** shown the base zone of 240 μm grit



**Fig. 9** SEM micrograph for Ti–6Al–4V alloy surface, **a** 240 μm, **b**, **c** 600 μm grit after the tribocorrosion test

in the smooth surface (600 μm) than in the rough surface (240 μm grit).

## 3.3 Chemical Composition Distribution After Tribocorrosion

Identification of chemical composition distribution for sample by EDS analysis after tribocorrosion for 600 μm grit at 25 N and 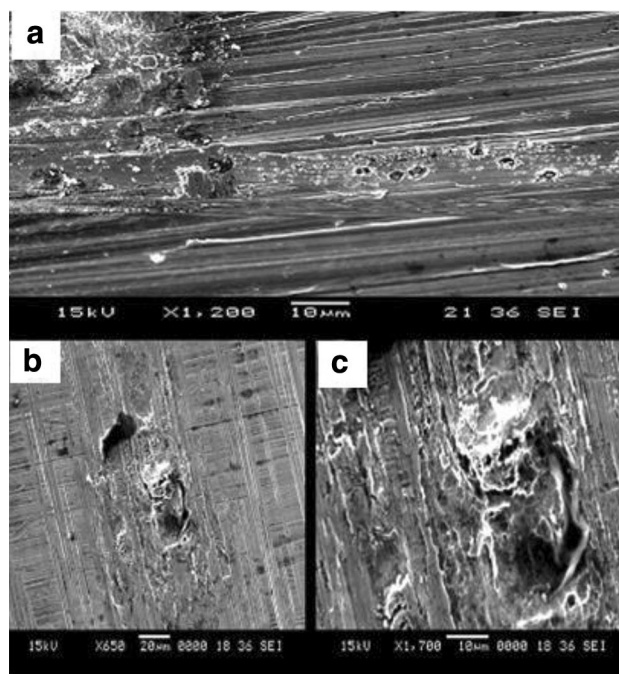for four zones, inside tribocorrosion area, outside tribocorrosion area, inside the pit and outside the pit as shown in Fig. 10, respectively. In addition to basic elements (Ti, Al, V) in alloy, (O, P, C, Cl, Ca) it is very clear in EDS analysis for these zones due to corrosion environment and chemical composition of PBS solution that use as electrolyte solution during tribocorrosion test.

## 3.4 Influence of Surface Roughness on Corrosion Rate

The open circuit potential (OCP) measurements depicts the influence of tribocorrosion: a decrease in OCP has been related to oxide film depassivation. During the potentiodynamic polarization test of 240 μm sample before and after tribocorrosion test, the corrosion potential decreases from −422 to −497 mV. Thus, the tribocorrosion current density increases from 3.85 to 4.95 μA/cm$^2$. The effect of rubbing on OCP (open circuit potential) is illustrated in Fig. 11, when the rubbing starts, OCP decreases due to a friction of magnitude. A third body plays a significant role. The third body could be ions, oxides, play a role in both fields: mechanics and corrosion. Moreover, the third body can consume some electrons, contribute to the global current measured, and lead to increased corrosion rates. The corrosion rate increases with increased surface roughness as the result to the increase in the current density. The corrosion rate before

**Fig. 10** EDS analysis of 600 μm grit surface at 25 N for: **a** inside fretting area, **b** outside fretting area, **c** inside the pit, **d** outside the pit
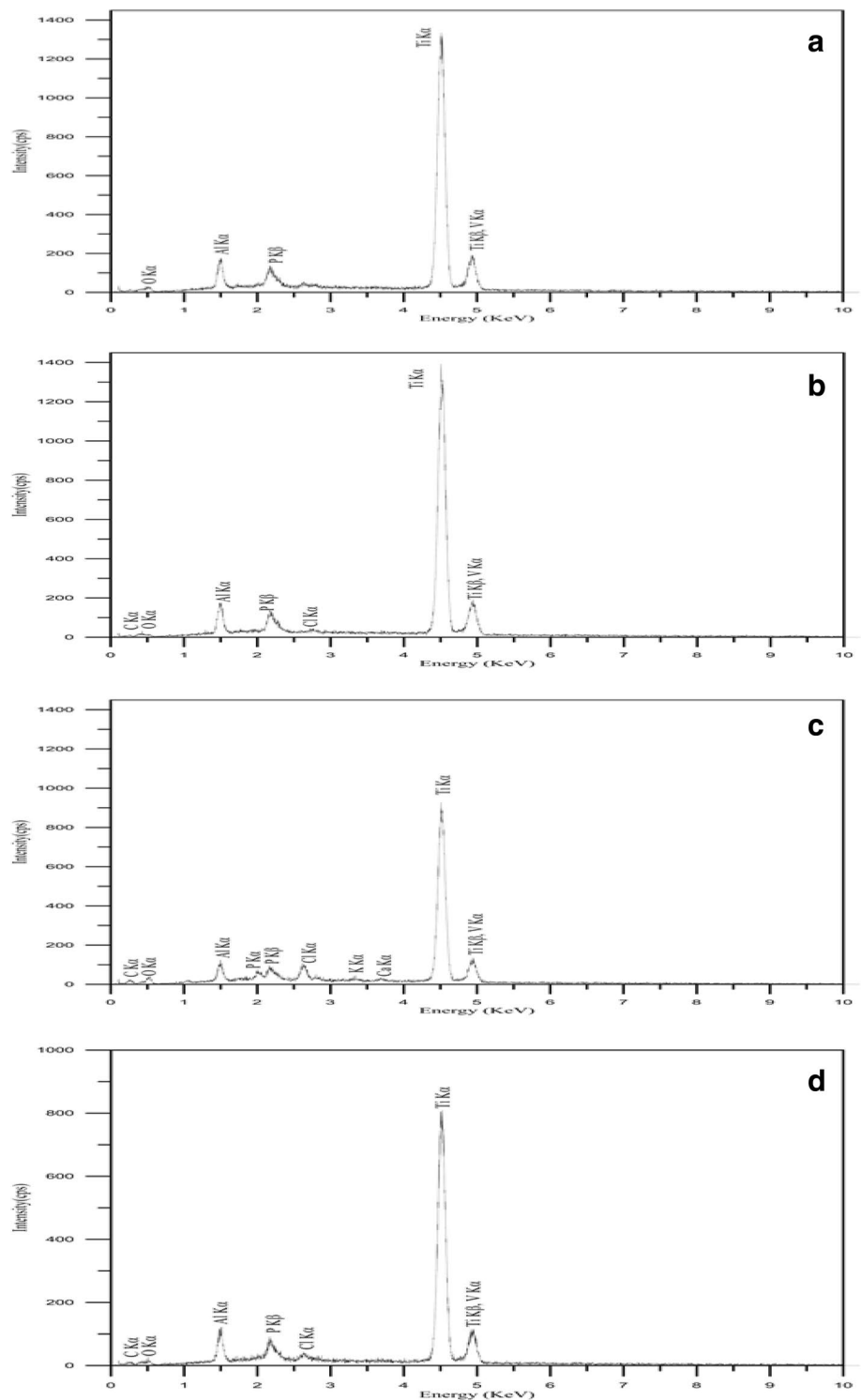


tribocorrosion tests lower than corrosion rate after tribocorrosion tests. The maximum corrosion rate at 240 μm grit while the minimum corrosion rate at 600 μm grit for both cases (before and after) tribocorrosion tests.

## 4 Conclusions

The current work focuses on investigating the effect of load and surface roughness on Ti–6Al–4V alloy during tribocorrosion corrosion tests. From the results of experimental work, the following conclusions have been derived:
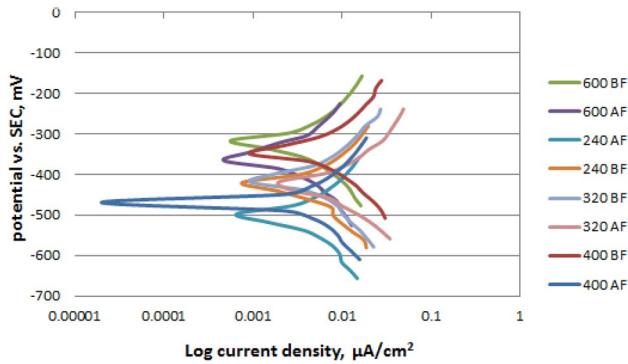
**Fig. 11** Comparable polarization curve among 240, 320, 400 and 600 μm grit samples before and after tribocorrosion tests

1. At initial load (0.5–8) N system, the current density increases with increase of load but at higher loads (8–25) N, the motion at the interface reduced and that lead to decrease the current density during tribocorrosion tests.

2. Tribocorrosion current density is depending on surface roughness. Due to oxide film depassivation, the higher Tribocorrosion current density is produced by the rough surface (240 μm grit), while the lower tribocorrosion current density are produced by the smooth surface (600 μm grit).

3. SEM results indicated that the plastic deformation and surface damage on smooth surface are more than that of rough surface. Fretting initiated crevice corrosion was obtained in both couples (smooth and rough). Crevice corrosion for smooth surface is more than crevice corrosion for rough surface.

4. OCP results indicated that the potential value for rough surface is greater than that of the potential value for smother surface (more electropositive). The corrosion rate increases after tribocorrosion tests.

5. EDS results show that the tribocorrosion area is affected by the environment and chemical composition of electrolyte solution.

# References

1. Liu W, Liu S, Wang L (2019) Surface modification of biomedical titanium alloy: micromorphology, microstructure evolution and biomedical applications. Coatings 249:1–23
2. Elias C, Lima J, Valiev R, Meyers M (2008) Biomedical applications of titanium and its alloys. Biol Mater Sci 60:46–49
3. Yazdi R, Ghasemi H, Abedini M, Wang C, Neville A (2018) Mechanism of tribofilm formation on Ti–6Al–4V oxygen diffusion layer in a simulated body fluid. J Mech Behav Biomed Mater 77:660–670
4. Li DG, Wang JD, Chen DR, Liang P (2015) Influence of molybdenum on tribo-corrosion behavior of 316L stainless steel in artificial saliva. J Bio and Tribo-Corros 2:1–14
5. Prando D, Brenna A, Vittroria M, Diamanti S, Beratta F, Bolzoni M Ormellease, Pia Pedeferri M (2017) Corrosion of titanium: part 1: aggressive environments and main forms of degradation. J Appl Biomater Funct Mater 15(4):291–302
6. Park J, Lakes R (2007) Biomaterials: an introduction. Springer Science & Business Media, Berlin
7. Lepicka M, Gradzka-Dahlke M (2016) Surface modification of Ti6Al4 V titanium alloy for biomedical applications and its effect on tribological performance—a review. Rev Adv Mater Sci 46(1):86–103
8. Yazdi R, Ghasemia H, Wangb C, Neville A (2017) Bio-corrosion behaviour of oxygen diffusion layer on Ti-6Al-4 V during tribocorrosion. Corros Sci 128:23–32
9. Gao A, Hang R, Bai L, Tang B, Chu PK (2018) Electrochemical surface engineering of titanium-based alloys for biomedical application. Electrochim Acta 271:699–718
10. Bailey R (2018) Tribocorrosion response of surface-modified Ti in a 0.9% NaCl solution. Lubricants 6(4):86
11. Huang W, Wang Z, Liu C, Yu Y (2015) Wear and electrochemical corrosion behavior of biomedical Ti–25Nb–3Mo–3Zr–2Sn alloy in simulated physiological solutions. J Bio Tribo-Corros 1(1):1–10
12. Licausi M, Munoz A, Borras V, Espallargas N (2015) Tribocorrosion mechanisms of Ti6Al4 V in artificial saliva by zero-resistance ammetry (ZRA) technique. J Bio Tribo-Corros 1(8):1–11
13. Chauhan S, Dass K (2013) Dry sliding wear behaviour of titanium (Grade 5) alloy by using response surface methodology. Adv Tribol 2013:1–9
14. Pejakovic V, Totolin V, Rodriguez Ripoll M (2018) Tribocorrosion behaviour of Ti6Al4 V in artificial seawater at low contact pressures. Tribol Int 119:55–65
15. Dimah M, Albeza D, Borras A (2012) Study of the biotribocorrosion behaviour of titanium biomedical alloys in simulated body fluids by electrochemical techniques. Wear 294:409–418
16. Licausi M, Igual A, Amig V (2013) Tribocorrosion mechanisms of Ti6Al4 V biomedical alloys in artificial saliva with different pHs. J Phys D 46:40
17. Mischler S (2008) Triboelectrochemical techniques and interpretation methods in tribocorrosion: a comparative evaluation. Tribol Int 41(7):573–583
18. Landolt D, Mischler S, Stemp M (2001) Electrochemical methods in tribocorrosion: a critical appraisal. Electrochim Acta 46:3913–3929
19. Mathew M, Srinivasa P, Pourzal R, Fischer A, Wimmer M (2009) Significance of tribocorrosion in biomedical applications: overview and current status. Adv Tribol 2009:1–12
20. Mathew M, Ariza E, Rocha L, Fernandes A, Vaz F (2008) TiCxOy thin films for decorative applications: tribocorrosion mechanisms and synergism. Tribol Int 41(7):603–615
21. Jamaati R, Reza M, Jerzy A, Duan L (2011) Tribocorrosion behavior of aluminium/alumina composite manufactured by anodizing and ARB processes. J Mater Eng Perform 20(9):1600–1605
22. Bryant M, Neville A (2017) Fretting corrosion of CoCr alloy: effect of load and displacement on the degradation mechanisms. Proc Inst Mech Eng [H] 231(2):114–126

23. Lopez-Ortega A, Arana J, Bayon R (2018) Tribocorrosion of passive materials: a review on test procedures and standards. Int J Corros 2018:1–24

24. Bailey R, Sun Y (2015) Corrosion and tribocorrosion performance of thermally oxidized commercially pure titanium in a 0.9% NaCl solution. J Mater Eng Perform 24(4):1669–1678

25. Mischler S, Barril S, Landolt D (2009) Fretting corrosion behaviour of Ti6Al4 V/PMMA contact in simulated body fluid. Tribol-Mater Surf Interfaces 3(1):16–23